71st Conference of the Italian Thermal Machines Engineering Association, ATI2016, 14-16 September 2016, Turin, Italy

Thermo-fluid dynamic analysis of a CSP solar field line during transient operation

Luca Migliari[a]*, Simone Arena[a], Pierpaolo Puddu[a], Daniele Cocco[a].

aUniversity of Cagliari, Department of Mechanical, Chemical and Materials Engineering - Via Marengo, 2 - Cagliari 09123, Italy

Abstract

Concentrating Solar Power (CSP) technology allows to produce high temperature thermal energy from solar radiation. The thermal energy can be converted into electricity or it can be directly used for industrial processes. Most of the available simulation models of CSP plants evaluate the behavior of the solar field in stationary conditions, neglecting transient thermo-fluid-dynamic effects. Nevertheless, the study of the dynamic behavior of the solar field is a very challenging and interesting task and allows obtaining useful information for the design and the effective management strategies of CSP plants. This paper presents a thermo-fluid-dynamic analysis of a solar field line of the CSP plant currently under construction in Ottana, Sardinia (Italy), which uses thermal oil as heat transfer fluid. Dynamics of the system due to solar irradiance variations have been evaluated by using an axisymmetric unsteady 2D numerical model developed in Comsol® to evaluate the oil temperature distribution along the receiver tube for different operating conditions. The results have been compared with those obtained with a simpler, non-stationary one-dimensional model, developed in Matlab® environment. The comparative analysis show very similar results for the two models and demonstrate that the dynamic effects on the temperature distribution along the solar field line are not negligible.

1. Introduction

Concentrating Solar Power (CSP) technologies produce high temperature thermal energy converting the beam component of solar radiation. Linear Fresnel Reflectors (LFR) are based on rows or loops of solar collectors using almost flat linear mirrors. Currently, more than 200 MW of CSP plants based on LFR are operating or under construction worldwide [1] but their use is extended also to direct thermal applications, e.g. industrial process heat or solar cooling. The worldwide interest in CSP is growing, and six EU countries had already included CSP in their National Renewable Action Plans [2]. The common element between thermal and electricity applications of concentrating solar technologies is the solar field. To the authors' knowledge, most of the scientific literature on the CSP solar fields is focused on steady state conditions. Referring to power generation, this is probably due to the frequent use of a Thermal Energy Storage (TES) section immediately downstream to the solar field, which essentially reduces the dynamic effects due to solar irradiance variations on the global plant response. However, a deep knowledge

* Corresponding author. Tel.: +39-070-675-5741.
   E-mail address: luca.migliari@unica.it

of the dynamic effects that occur along the solar field is of great interest, and some studies have been already carried out on the optimal design [3], effective control strategies and predictive management [4][5] of CSP plants considering dynamics. When solar concentrators are used for thermal applications, a direct usage of the process heat usually occurs and no TES section is included. In this case, the softening function of the TES section is totally absent and consequently the dynamic effects could be relevant.

This paper presents a thermo-fluid-dynamic analysis of a solar field line of the Solar Power Plant currently under construction in Ottana, Sardinia (Italy), which combines CSP and CPV (Concentrating Photo-Voltaic) technologies in order to improve the dispatchability of solar power plants [6]. To evaluate different system management methods, the availability of simple and agile simulation models are of great importance. For this reason, the aim of this paper is to assess the reliability and applicability of a non-stationary one-dimensional model developed in Matlab® for the simulation of the solar field through the comparison with a more sophisticated unsteady 2D numerical model developed under Comsol®.

Nomenclature

Symbols

A	area, m2
c_p	specific heat at constant pressure, J/(kg·K)
C	thermal capacity, J/K
D	diameter, m
h	convective heat transfer coefficient, W/(m2·K)
k_c	conductive heat transfer coefficient, W/(m·K)
$\dot{m}$	mass flow rate, kg/s
P	pressure, Pa
$\dot{q}$	thermal power, W
S	surface, m
t	time, s
T	temperature, °K
u	velocity, m/s
$\dot{w}$	shaft power, W

ε	turbulent dissipation rate
η_{opt}	optical efficiency
μ	dynamic viscosity, Pa·s
ρ	density, kg/m3

Subscripts

env	environment
ext	external
f	fluid
int	internal
r	reference
s	shaft
t	tube
T	turbulent

1.1. Characteristics of the solar field

The solar field of the Ottana power plant is composed of 6 lines of Linear Fresnel collectors, each 200-meter-long, and connected in a central feed configuration. The solar field uses a Dowtherm®-T thermal oil as heat transfer fluid, with a design inlet temperature of 150°C, an outlet temperature of 260°C and a rated total mass flow of 17.3 kg/s (the design conditions are DNI 900 W/m^2, air temperature 17 °C, elevation 73°, azimuth 0°). Further information about main operating parameters and assumptions can be found in Table 1.

The Archimede HCEOI12 receiver tube here considered (Fig. 1) is commercially available and its characteristics can be found in [7]. It is composed of an internal longitudinally electric-welded austenitic stainless steel tube with lapped external surface (thickness 2 mm). An external borosilicate glass of 3 mm thickness protects the tube and its anti-reflective coating treatment allows a transmittance of solar radiation higher than 96.6%. The thermal emissivity of the spectrally selective coating is about 8.5% at 400°C. Between the steel tube and the glass cylinder, a vacuum annulus is created in order to reduce the convective heat losses. Several tubes are connected in series through special bellow couplings to form a receiver line. Each line is supported by a rail, which allows its thermal expansion along the axis.
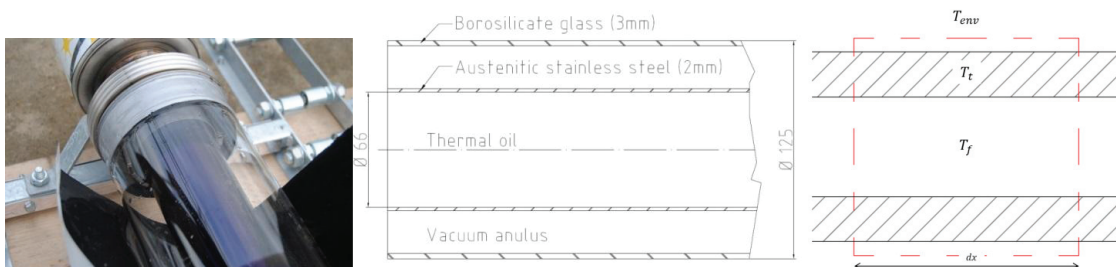

Fig. 1. Archimede HCEOI12 receiver tube and the control volume considered in 1D model.

Table 1 - Main operating parameters and assumptions regarding the solar field.

Solar field			
Collecting area, Ac	8,400 m^2	Cleanliness efficiency	98%
Land area	10,800 m^2	Oil inlet / outlet temp.	150/260 °C
Line length	200 m	Thermal oil mass flow	17.3 kg/s
Thermal oil (DOWTHERM T)			
Density	763 kg/m^3	Specific heat at constant pressure	2439.4 J/(kg·K)
Thermal conductivity	0.110 W/(m·K)	Dynamic viscosity	0. 5 mPa·s
Receiver Tube (AISI 304 – austenitic stainless steel)			
Reference optical efficiency, $\eta_{opt,r}$	62%	Specific heat	0.50 kJ/(kg·K)
Density	8030 kg/m^3	a$_1$ thermal losses coefficient (eq.(7))	0.056 W/m^2·K
Thermal conductivity	20 W/(m·K)	a$_2$ thermal losses coefficient (eq.(7))	2.13·10-4 W/m^{2}K^2

The Dowtherm®-T thermal oil has a composition based on C14 to C30 alkyl benzene derivatives. Its optimal operating temperature range is (-10°C - 288°C) and it is designed for use in non-pressurized systems.

2. System modeling and assumptions

2.1. Non- stationary one-dimensional model

The one-dimensional mathematical model is based on the mass, momentum and energy conservation equations applied to the control volume shown in Fig. 1. A very simplified version of the model, without dynamic effect contributions, was previously developed by the authors [8]. The resulting energy and mass balance equations are:

$$\frac{\partial}{\partial t}\left[\rho A \left(e + \frac{u^2}{2} + gz\right)\right] dx + \frac{\partial}{\partial x}\left[\rho u A \left(e + \frac{u^2}{2} + \frac{P}{\rho} + gz\right)\right] dx = \dot{w}_s + \dot{q}_{sun} \tag{1}$$

$$\frac{\partial}{\partial t}(\rho A) + \frac{\partial}{\partial x}(\rho u A) = 0 \tag{2}$$

In the present study, the kinetic and potential energy terms have been neglected, shaft work exchanged by the control volume is zero, no mass accumulation occurs inside each control volume ($\rho = const$), and a constant cross section area was considered. The model has been discretized considering three sub-systems characterized by the following thermal state: environment T_{env}, tube T_t and fluid T_f. Eq. (1) applied to fluid and receiver tube is reported in Eqs. (3) and (4)

$$C_f \frac{dT_f}{dt} = R_{t,f}\left(T_t - T_f\right) - \dot{m} c_{p,f} \frac{\partial T_f}{\partial x} dx \tag{3}$$

$$C_t \frac{dT_t}{dt} = \dot{q}_{sun} - \dot{q}_{loss} - R_{t,f}\left(T_t - T_f\right) - k_{c,t} A \frac{\partial T_t}{\partial x} \tag{4}$$

where R$_{t,f}$ is the equivalent thermal conductance between tube and fluid, which is calculated as:

$$R_{t,f} = h_{t,f}\,\pi D_{t,int} dx \tag{5}$$

The $h_{t,f}$ convective heat transfer coefficient is obtained from the Dittus-Boelter equation, under the hypothesis of a turbulent flow ($Re \gtrsim 10000$), Prandtl number range ($0.6 \leq Pr \leq 160$), $L/D \gtrsim 10$ and a smooth inner tube surface:

$$Nu = 0.023 \, Re^{0.8} Pr^n \tag{6}$$

where n = 0.4 if T$_t$ > T$_f$ and n = 0.3 elsewhere.

The term $\dot{q}_{loss}$ of eq. (4) represents the thermal losses of the receiver tube and is calculated as:

$$\dot{q}_{loss} = a_1(T_t - T_{env}) + a_2(T_t - T_{env})^2 \tag{7}$$

where a$_1$ and a$_2$ are given by the manufacturer data sheet.

The thermal power concentrated by mirrors on the receiver tube is evaluated through the following equation:

$$\dot{q}_{sun} = A_c \, DNI \, \eta_{opt,r} \, IAM_L \cdot IAM_T \, \eta_{CLN} \tag{8}$$

where IAM_L and IAM_T are the longitudinal and transversal components of the incidence angle modifier factor and η_{CLN} is the surfaces cleanliness factor. The two correction factors IAM_L and IAM_T considered in this study are reported in [8].

2.2. Non-stationary two-dimensional model

A 2D axisymmetric numerical model has been developed in the COMSOL Multiphysics platform to simulate the solar field line. The system has been modeled considering the thermo-fluid dynamics behavior of the entire domain. The domain was reported in Fig. 2(a) and discretized using a structured mesh Fig. 2(b) composed of 10^5 elements with maximum size of 10 mm.

The physical time of the simulations using COMSOL Multiphysics platform was 2590 s, while the duration of the simulation (real time) on a ASUS workstation with I7 Quad-Core CPU and 16 GB memory was 3600 s. No appreciable differences in the results were observed using finer meshes and shorter time steps.
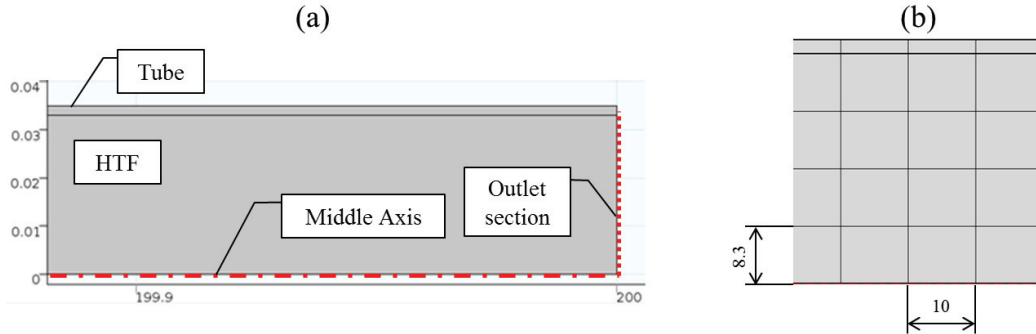

Fig. 2.Domains of the 2D model (a) and particular of the mesh adopted (b).

The axial temperature evolution of the HTF over the time was evaluated along the dash-dot red line shown in Fig. 2, which represents the axisymmetric line of the domain. The temperature evolution at solar field outlet was evaluated at the intersection point between the red dash-dot and the red dotted line of Fig. 2(a), representing the central point of the outlet section.

Reynolds-Averaged Navier-Stokes (RANS) equations based on k-ε turbulence model were used to solve the flows through the solar receiver. Continuity eq. (9) and momentum (eq. 10) equations are coupled with two additional transport equations involving the turbulent kinetic energy, k (eq. (11)), and the turbulent dissipation rate, ε (eq. (12)). The turbulent viscosity is defined by eq. (13):

$$\frac{\partial \rho_f}{\partial t} + \nabla \cdot \left(\rho_f u_f\right) = 0 \tag{9}$$

$$\rho_f \frac{\partial u_f}{\partial t} + \rho_f (u_f \cdot \nabla) u_f = \nabla \cdot \left[-P_f l + \left(\mu_f - \mu_{T,f}\right)\left(\nabla u_f + \left(\nabla u_f\right)^T\right) - \frac{2}{3}\left(\mu_f - \mu_{T_f}\right)\left(\nabla \cdot u_f\right)l - \frac{2}{3}\rho_f kl\right] \tag{10}$$

$$\rho_f \frac{\partial k}{\partial t} + \rho_f (u_f \cdot \nabla) k = \nabla \cdot \left(\left(\mu_f + \frac{\mu_{T,f}}{\sigma_k}\right)\nabla k\right) + P_k - \rho_f \varepsilon \tag{11}$$

$$\rho_f \frac{\partial \varepsilon}{\partial t} + \rho_f (u_f \cdot \nabla)\varepsilon = \nabla \cdot \left(\left(\mu_f + \frac{\mu_{T,f}}{\sigma_\varepsilon}\right)\nabla \varepsilon\right) + C_{\varepsilon 1}\frac{\varepsilon}{k}P_k - C_{\varepsilon 2}\rho_f \frac{\varepsilon^2}{k} \tag{12}$$

$$\mu_{T_f} = \rho_f C_\mu \frac{k^2}{\varepsilon} \tag{13}$$

where $e_t = \left(e_{t,x} e_{t,y} e_{t,z}\right)$ is the unit tangent vector to the pipe axis, l is the mixing length, C_μ, $C_{\varepsilon 1}$, $C_{\varepsilon 2}$, σ_k, σ_ε are dimensionless model constants [9] [10], and k is the turbulence kinetic energy.

The production term P_k, which represents the rate at which kinetic energy is transferred from the mean flow to the turbulence, is given by eq. (14):

$$P_k = \mu_{T,f}\left(\nabla u_f : \left(\nabla u_f + \left(\nabla u_f\right)^T\right) - \frac{2}{3}\left(\nabla \cdot u_f\right)^2\right) - \frac{2}{3}\rho_f k \nabla \cdot u_f \tag{14}$$

In order to simulate the heat transfer that occurs in the entire domain, the energy equation (15) was used:

$$\rho C_p \frac{\partial T}{\partial t} + \rho C_p u \cdot \nabla T = \nabla \cdot (k_c \nabla T) + q_{conv} \tag{15}$$

To simulate the heat solar power, the boundary condition in the outer wall of the solar receiver was assumed as a net heat flux $(\dot{q}_{sun} - \dot{q}_{loss})/S_t = -n \cdot (-k_c \nabla T)$ where S is the total area of this boundary. The heat transfer inside the tube is characterized by conduction while the heat transfer between the tube and the HTF occurs both via conduction and

convection. The energy equation (eq.(15)) applied to the HTF is solved using the velocities calculated from eqs. (9) and (10), in order to evaluate the interactions between fluid dynamics and heat transfer phenomena. The specific thermal power q_{conv} takes into account the convective heat transfer between fluid and internal wall of the receiver.

3. Results

The comparison between the two developed models has been carried out with reference to three different operating conditions of the solar field:
a) the warm-up phase, obtained simplifying the increasing power coming from the sun after sunshine with ramps of different duration;
b) the full operation transients, applying different steps and pulses of the sun power;
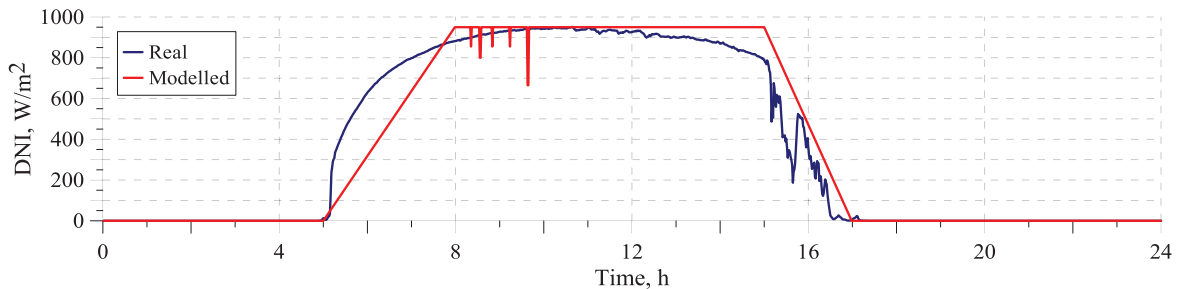c) the shut-down phase, realized through a ramp with a negative slope (Fig. 3).

Fig. 3. Real and modelled trend of DNI.

3.1. *Warm-up phase*

This phase occurs immediately after sunshine, and it was modeled through different ramps of power coming from the sun (Q_{sun}). Two, three and four-hour long Q_{sun} ramps have been considered, starting from zero and up to the design power ($Q_{sun, design} \approx 720$ kW), obtained with a DNI value of 900 W/m^2, an air temperature of 17 °C, an elevation of 73° and an azimuth of 0°. The HTF flows from the cold tank (T=150°C), with a constant mass flow of 0.5 kg/s (about 17% of the nominal mass flow value) and without recirculation through the solar field. The HTF and tube temperatures were initially set equal to the environment temperature (17°C).

Fig. 4(a) shows the fluid temperature at the SF outlet over the time, for the three cases of 2, 3 and 4-hour-long ramps of Q_{sun}. For each case, the evolution of the temperature at the outlet of the SF over the time can be virtually subdivided in three parts. The first part (with the lowest slope rate) shows the little increase of the temperature at the outlet of the SF mainly caused by the temperature difference between fluid and tube, which is heated by the available sun radiation. In fact, during the first 10-15 minutes, the contribution of the mass transport term of eq. (3) significantly affects only the positions immediately downstream of the duct inlet, due to the great distance between the inlet and outlet tube sections. During the second very sloped part of each curve, the influence of the mass transport term at the outlet section of the SF is stronger. Finally, during the third and last part of the warm-up curve, the temperature trend slope is again reduced, for the smaller temperature gradient between adjacent sections. Different durations are required for the entire warm-up process up to 260°C, in accordance with the DNI ramps: with a ramp of two hours, the outlet design temperature is reached approximately after 40 minutes, with a three-hour long ramp more than 50 minutes are required and with a four-hour long ramp the warm-up process takes more than one hour.

Fig. 4(b) shows the progressive evolution of the temperature distribution along the solar field line, for the case of the 2-hour long ramp. Comparison of the right sections of the 5 minutes and 10 minutes curves highlights the negligible contribution of the mass transport term of eq. (3) at the farthest segments of the duct, at these moments. It's interesting to notice that, even after the second inflection point of Fig. 4(a), the temperature distribution shown in Fig. 4(b) is not linear during transient, but it becomes linear only at equilibrium. The comparison between the results of the two simulation models gives very close curves, with little differences only around the first inflection point of Fig. 4(a) (as highlighted in the sub-graphs) and around the second inflection point of Fig. 4(b).
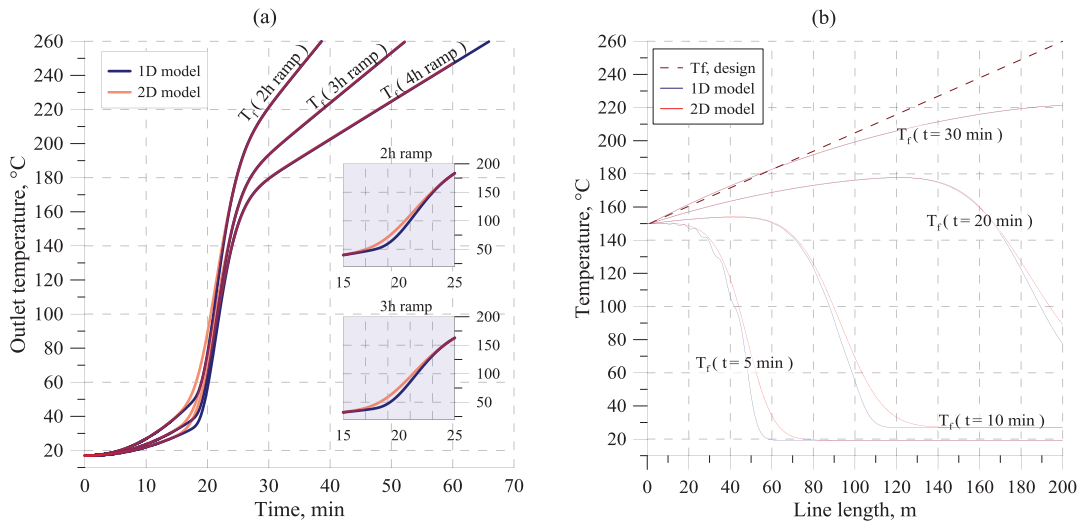
Fig. 4. Outlet temperature of the SF(a) and temperature distribution along the SF line for the case of 2-hour long ramp (b).

3.2. *Full-operation transients*

Since concentrating solar technologies use only the direct component of the global irradiance (DNI), during the solar field operating phase the clouds' passage over the mirrors causes frequent variations of the receiver tube available power. These variations can be sudden or gradual and brief or long-lasting: in fact the DNI can widely vary its value even down to zero in few seconds. For this reason, the two models' responses to Q_{sun} steps and rectangular pulses of different amplitude and duration are shown and described in the present paragraph.
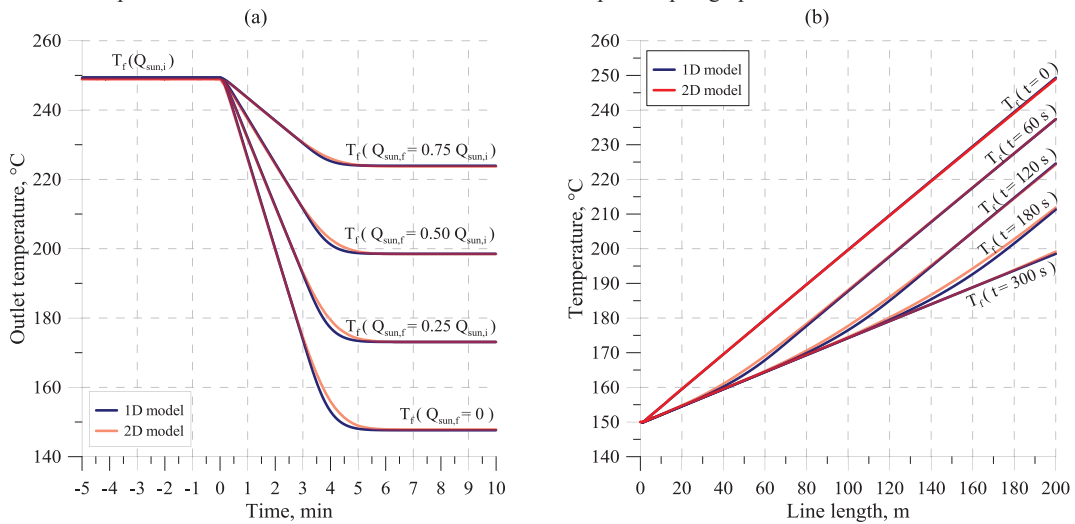

Fig. 5. Fluid temperature at the outlet of the SF(a) and temperature distribution along the SF line for the case of final DNI=50%(b).

Fig. 5(a) shows the system responses when a Q_{sun} step occurs: the Q_{sun} amplitude suddenly decreases by 25%, 50%, 75% and 100%, starting from the nominal conditions. As it can be seen, the two developed models lead to very similar results. Each step in Q_{sun} determines a new equilibrium condition of the system after approximately 6 minutes of the step occurrence, and the final equilibrium temperature depends on the final Q_{sun} amplitude. For a final Q_{sun} amplitude of 25%, the outlet final temperature is about 175°C, while for a final Q_{sun} amplitude of 50% the value is slightly above 200°C and for a final Q_{sun} of 75% the HTF temperature is around 225°C. If the final Q_{sun} is zero, as shown, the HTF thermal exchanges are only represented by heat losses, so the final equilibrium temperature is a little below the inlet temperature of 150°C. The temperature distribution along the line and its evolution over time can be seen in Fig. 5(b). T_f (t=0) shows the initial equilibrium condition: the temperature distribution along the line can be represented by a

straight line. One minute after the step occurrence the slope is reduced and an inflection point occurs. The inflection point moves along the line until a new equilibrium condition is reached and the temperature distribution returns to be linear.

During real operating conditions of a solar field, Q_{sun} variations in the range of 10-30% are very frequent and they can be modeled through rectangular pulses. Fig. 6 (a-f) show the system responses to Q_{sun} pulses of different amplitude and durations operating at the nominal mass flow rate condition. This operating condition has been considered in order to determine a threshold level for the regulation action of the circulating pumps: in fact, if the Q_{sun} variation causes negligible variations of the outlet temperature, the oil mass flow can be maintained constant. Fig. 6 (a), (b), (c) show system responses to pulses starting at t=0 and having the same duration (t=60s) but different amplitudes ($Q_{sun,f}$ = 0.9 $Q_{sun,i}$, $Q_{sun,f}$ = 0.8 $Q_{sun,i}$, $Q_{sun,f}$ = 0.7 $Q_{sun,i}$). Fig. 6 (d), (e), (f) show responses to pulses starting at t=0 and having a longer duration (t=90s) and amplitudes of $Q_{sun,f}$ = 0.9 $Q_{sun,i}$, $Q_{sun,f}$ = 0.8 $Q_{sun,i}$, $Q_{sun,f}$ = 0.7 $Q_{sun,i}$, correspondingly.
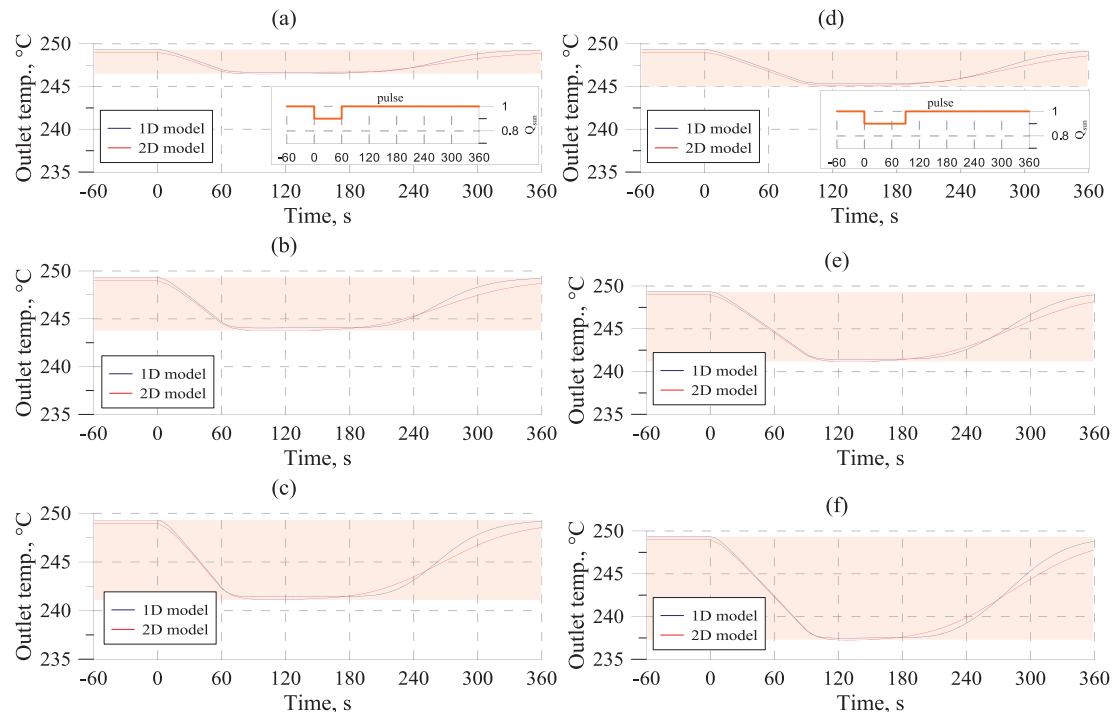

Fig. 6. Outlet temperature of the SF: system responses to pulses. (a) $Q_{sun,f}$ = 0.9 $Q_{sun,i}$, t=60s; (b) $Q_{sun,f}$ = 0.8 $Q_{sun,i}$, t=60s; (c) $Q_{sun,f}$ = 0.7 $Q_{sun,i}$, t=60s; (d) $Q_{sun,f}$ = 0.9 $Q_{sun,i}$, t=90s; (e) $Q_{sun,f}$ = 0.8 $Q_{sun,i}$, t=90s; (f) $Q_{sun,f}$ = 0.7 $Q_{sun,i}$, t=90s.

Results of Fig. 6 demonstrate that the temperature drop increases with the increase of both amplitude and duration of the pulse. A 10% decrease of the solar power input lasting up to 90s (Fig. 6 (a) and (d)), causes temperature drops in the range of 5°C. In the case of a deeper Q_{sun} decrease (20%), Fig. 6(b) and (e) show that the temperature fall can be almost doubled (10°C), in the case of 90s pulse, with respect to the aforementioned cases. The case of a 30% Q_{sun} reduction is reported in Fig. 6(b) and (e) and gives a maximum temperature drop of about 15°C. Fig. 6 also demonstrates that the results obtained through the 1D and 2D models are very close and similar, especially during the temperature decreasing phase.

3.3. *Shut-down phase*

The shut-down phase is the operating condition of the solar field during the final daily time, which occurs before sunset and has been modeled trough a Q_{sun} negative ramp, which starts from $Q_{sun, design}$ down to zero in 2 hours, at the nominal mass flow rate. Fig. 7(a) shows the solar field outlet temperature over time. The outlet temperature linearly decreases and with the considered input power Q_{sun}, the minimal temperature of 150°C is reached after two hours.
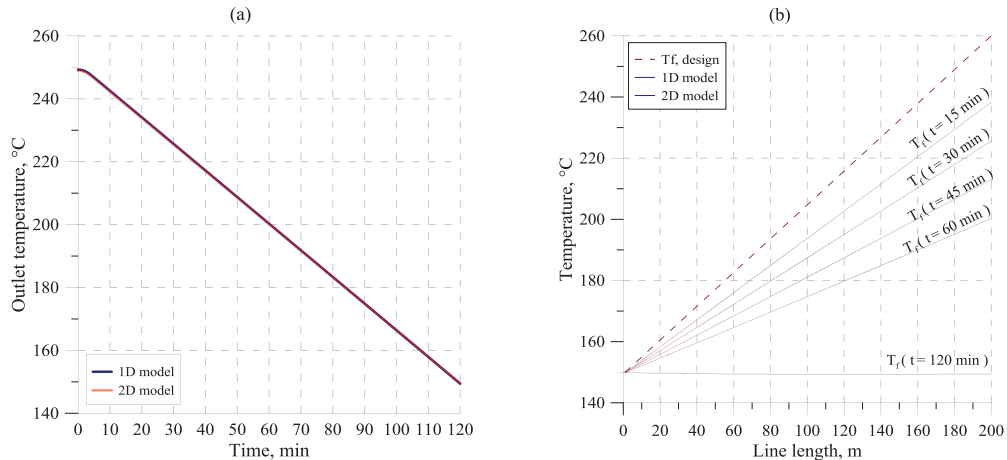
Fig. 7. Outlet temperature of the SF(a) and temperature distribution along the SF line for the shut-down phase(b)

4. Conclusions

The present work investigated the dynamic responses of a solar field line of the CSP section of the Ottana Solar Power Plant. Furthermore, a comparison between a non-stationary one-dimensional model and a non-stationary two dimensional model has been carried out. Three operating phases of the solar field line have been studied: warm-up, full operation transients and shut-down phases. Depending on the time evolution of the solar power, the warm-up process up to nominal conditions can last up to more than 1 hour, and the temperature distribution along the line evolves with some inflection points that gradually disappear. The full operation transients have been modeled through steps and pulses of different amplitude and duration. The most important conclusion of this phase analysis is that a time period of about 5-6 minutes after the step/pulse occurrence is necessary to restore new equilibrium conditions. The shut-down phase analysis allows knowing the system response to a decreasing ramp of incoming solar power. The two models lead to very similar dynamic responses for all three operating phases. For this reason, the simplified one-dimensional model can be confidently used for control and management purposes.

The results discussed in this paper will be experimentally validated once the construction of the Ottana Solar Hybrid Power Plant will be completed. Thereafter, since the effectiveness of the simplified one-dimensional model has been assessed by the present study, this simulation model can be reliably used to evaluate and compare different energy management strategies of the CSP system.

References

[1]   SolarPACES, Greenpeace, Estela. Solar Thermal Electricity Global Outlook 2016. 2016.
[2]   Strategic Energy Technologies Information System (SETIS). Concentrated solar power 2014.
[3]   Luo N, Yu G, Hou HJ, Yang YP. Dynamic Modeling and Simulation of Parabolic Trough Solar System. Energy Procedia 2015;69:1344–8.
[4]   Stuetzle T. Automatic Control of the 30 MWe SEGS IV Parabolic Trough Plant 2002.
[5]   Forristall R. Heat Transfer Analysis and Modeling of a Parabolic Trough Solar Receiver Implemented in Engineering Equation Solver 2003:164.
[6]   Cocco D, Migliari L, Petrollese M. A hybrid CSP–CPV system for improving the dispatchability of solar power plants. Energy Convers Manag 2016;114:312–23.
[7]   Archimede Solar Energy - HCEOI12 n.d. http://www.archimedesolarenergy.it/en_hceoi-12-olio.htm (accessed March 23, 2016).
[8]   Migliari L, Arena S. Thermal Energy Losses During Night, Warm-up and Full-Operation Periods of a CSP Solar Field Using Thermal Oil. Energy Procedia 2015;82:1002–8.
[9]   Comsol. The Heat Transfer Module User's Guide.
[10]   Rolander N, Rambo J, Joshi Y, Allen JK, Mistree F. An Approach to Robust Design of Turbulent Convective Systems. J Mech Des 2006;128:844–55.